Opening of the Blood–Brain Barrier Using Low-Intensity Pulsed Ultrasound Enhances Responses to Immunotherapy in Preclinical Glioma Models

Aria Sabbagh[1], Kevin Beccaria[1,2], Xiaoyang Ling[1], Anantha Marisetty[1], Martina Ott[1], Hillary Caruso[1], Emily Barton[3], Ling-Yuan Kong[1], Dexing Fang[1], Khatri Latha[1], Daniel Yang Zhang[4], Jun Wei[1], John DeGroot[5], Michael A. Curran[6], Ganesh Rao[1], Jian Hu[7], Carole Desseaux[8], Guillaume Bouchoux[8], Michael Canney[8], Alexandre Carpentier[9,10], and Amy B. Heimberger[1]

ABSTRACT

Purpose: The blood–brain barrier (BBB) inhibits adequate dosing/penetration of therapeutic agents to malignancies in the brain. Low-intensity pulsed ultrasound (LIPU) is a safe therapeutic method of temporary BBB disruption (BBBD) to enhance chemotherapeutic delivery to the tumor and surrounding brain parenchyma for treatment of glioblastoma.

Experimental Design: We investigated if LIPU could enhance therapeutic efficacy of anti–PD-1 in C57BL/6 mice bearing intracranial GL261 gliomas, epidermal growth factor receptor variant III (EGFRvIII) chimeric antigen receptor (CAR) T cells in NSG mice with EGFRvIII-U87 gliomas, and a genetically engineered antigen-presenting cell (APC)-based therapy producing the T-cell attracting chemokine CXCL10 in the GL261-bearing mice.

Results: Mice treated with anti–PD-1 and LIPU-induced BBBD had a median survival duration of 58 days compared with 39 days for mice treated with anti–PD-1, and long-term survivors all remained alive after contralateral hemisphere rechallenge. CAR T-cell administration with LIPU-induced BBBD resulted in significant increases in CAR T-cell delivery to the CNS after 24 ($P < 0.005$) and 72 ($P < 0.001$) hours and increased median survival by greater than 129%, in comparison with CAR T cells alone. Local deposition of CXCL10-secreting APCs in the glioma microenvironment with LIPU enhanced T-cell glioma infiltration during the therapeutic window ($P = 0.004$) and markedly enhanced survival ($P < 0.05$).

Conclusions: LIPU increases immune therapeutic delivery to the tumor microenvironment with an associated increase in survival and is an emerging technique for enhancing novel therapies in the brain.

Introduction

Currently, a large compendium of immune therapeutics, including immune-checkpoint inhibitors, immune modulators, and cellular therapeutics, is hindered by a lack of BBB penetration. As previously described, these immunotherapies may lack antitumor activity either by an inability to interact within the glioma microenvironment or by a paucity of immune-effector trafficking (1). CNS detection of peripherally administered antibodies is less than 1% (2). Although some antibodies may be modified for increased CNS delivery, this strategy may not be applicable for other therapeutics. Some immune cells like macrophages are abundant in gliomas (3, 4), while cytolytic immune cells like T and natural killer cells are scarce (5). Additionally, intracranial tumors can further deplete T cells through sequestration in the bone marrow (6). Therefore, immune-checkpoint inhibitors may lack function even if they are adequately delivered to the tumor microenvironment. Novel methods must be investigated for increasing T-cell infiltration and activity at the tumor site.

BBB opening using low-intensity pulsed ultrasound (LIPU) is a favorable method for facilitating the delivery of various therapeutics, such as antibodies and cells, into the glioma microenvironment (7–9). Antibodies that act in the CNS may gain an advantage by being better delivered through LIPU-induced BBB opening. These antibodies could act on targets like tumor antigens or cell populations like microglia, which are present in the CNS. LIPU-induced BBB opening may not add therapeutic value if the primary action of an immunotherapy is in the periphery and there is already sufficient access to the tumor microenvironment by immune-effector cells. Also important is ascertaining whether LIPU can improve other immunotherapies by enhancing the presence of effector cells at the site of the tumor. By increasing immune cell delivery to the tumor microenvironment, an immunologically "cold" tumor may be converted into an immunologically "hot" one, and this may further potentiate immune-checkpoint inhibitor strategies. Adoptive immunotherapies for brain tumors, such as chimeric antigen receptor (CAR) T cells, natural killer cells, and adoptive T cells have been limited by a lack of sufficient

[1]Department of Neurosurgery, The University of Texas MD Anderson Cancer Center, Houston, Texas. [2]Department of Pediatric Neurosurgery, Hôpital Necker-Enfants Malades, APHP, Université de Paris, 75015 Paris, France. [3]Department of Psychology and Behavioral Neuroscience, St. Edward's University, Austin, Texas. [4]Department of Neurosurgery, Northwestern University, Chicago, Illinois. [5]Department of Neuro-Oncology, The University of Texas MD Anderson Cancer Center, Houston, Texas. [6]Department of Immunology, The University of Texas MD Anderson Cancer Center, Houston, Texas. [7]Cancer Biology, The University of Texas MD Anderson Cancer Center, Houston, Texas. [8]CarThera, Institut du Cerveau et de la Moelle épinière, Paris F-75013, France. [9]AP-HP, Neurosurgery Department, Pitie Salpetriere Hospital, F-75013 Paris, France. [10]Sorbonne Universite, GRC23, Interface Neuro Machine team, F-75013 Paris, France.

Note: Supplementary data for this article are available at Clinical Cancer Research Online (http://clincancerres.aacrjournals.org/).

A. Sabbagh and K. Beccaria contributed equally to this article.

Corresponding Author: Amy B. Heimberger, Northwestern University, Feinberg School of Medicine, Simpson Querrey Biomedical Research Center, 303 E. Superior Street, 6-516, Chicago, IL 60611. Phone: 312-503-3805; E-mail: Amy.heimberger@northwestern.edu

Clin Cancer Res 2021;27:4325–37

doi: 10.1158/1078-0432.CCR-20-3760

Translational Relevance

Our studies showed that low-intensity pulsed ultrasound (LIPU)-induced blood–brain barrier disruption (BBBD) can enhance the therapeutic effects of a variety of immunotherapeutic strategies for glioblastoma by enhancing delivery of antibodies, CAR T cells, and genetically modified cellular immunotherapeutics to the tumor microenvironment. With increasing numbers of clinical studies showing the safety of LIPU-induced BBBD, this technique could be rapidly translated to clinical trials in association with immune therapeutic strategies.

delivery to the CNS. Therefore, ultrasound may be a reversible and safe method of BBBD for delivery of multiple doses of immunotherapeutics to targeted brain regions. LIPU-mediated BBBD may also be considered for delivering benign cells elaborating immune cytokines or chemokines to modulate local tumor immune responses. If these cells are capable of antigen presentation, this strategy could stimulate T cells at the site of the tumor. In addition, disruption of the BBB may also release tumor antigens into the peripheral circulation, which could activate peripheral antigen-presenting cells (APCs). As such, LIPU-mediated BBBD is an emerging technology that provides multiple avenues for enhancement of immunotherapy for glioma treatment. For this study, we hypothesized that, in preclinical models of glioblastoma, LIPU-induced opening of the BBB would further enhance the therapeutic impact of a wide variety of immune therapeutics that have either been tested in glioblastoma patients and failed or a novel cellular strategy that demonstrated no evidence of efficacy previously. The purpose of this translational study was to assess the specific types of immunotherapy that could be considered for use in clinical trials of BBBD with LIPU.

Materials and Methods

Cell culture

Murine glioblastoma stem cells lines derived from *Nestin-CreER^{T2} Qk$^{L/L}$; Trp53$^{L/L}$; Pten$^{L/L}$* mice (QPP) were provided as a gift from Dr. Michael Curran and Jian Hu (The University of Texas MD Anderson Cancer Center). QPP4 cells were cultured in DMEM/F12 media with B-27 supplement (Gibco), epidermal growth factor (EGF), and fibroblast growth factor (FGF; STEMCELL Technologies; ref. 10). Murine GL261 and human U87 glioma cell lines were purchased from the NIH. U87 cells were transfected with epidermal growth factor receptor variant III (EGFRvIII) and were provided as a gift from Dr. Oliver Bogler (The University of Texas MD Anderson Cancer Center). U87 and GL261 cell lines were maintained in Dulbecco's modified Eagle's medium (Life Technologies) supplemented with 10% fetal bovine serum (Gibco) and 1% penicillin/streptomycin at 37° C in a humidified atmosphere of 5% CO_2 and 95% air. Cells were trypsinized for 3 minutes at 37°C and neutralized with a medium containing fetal bovine serum at a 1:5 dilution.

LIPU preclinical platform

The LIPU preclinical platform (SonoCloud Technology, CarThera) consists of an ultrasound transducer placed in a small cylinder surrounded by a compartment of degassed water to ensure acoustic coupling. A laser is vertically aligned on the center of the transducer. To enhance reproducibility of the sonicated areas of the brain, the mouse's shaved head is placed in contact with the surface of the degassed water and the area of tumor implantation is aligned with the laser dot. Head stabilization allows for motionless sonication to the CNS (**Fig. 1A**). The transducer used a center frequency of 1-MHz, pulse-repetition frequency of 1 Hz, pulse length of 25,000 cycles (2.5% duty cycle), and *in situ* acoustic pressure level of 0.3 MPa for a duration of 120 seconds. A 200-μL bolus of microbubbles (Lumason, Bracco Diagnostics) was injected through the tail vein just prior to the start of sonications. These were safe parameters as determined in previous experiments in mice (11).

Ultrasound-induced BBBD procedures

For all LIPU procedures, hair was removed from mice's heads with a clipper and hair removal cream (Nair) on the day before the first treatment. Sonications of mice were performed under general anesthesia after intraperitoneal injection of 150 to 200 μL of a mixture of 10 mg/kg xylazine (AnaSed; Akorn, Inc.) and 100 mg/kg ketamine HCl (Henry Schein). The feasibility and reproducibility of LIPU-induced BBBD was assessed with the diffusion of Evans blue dye (Sigma-Aldrich; ref. 12), which binds to albumin and does not freely cross the intact BBB (13). The dye was diluted in saline, and 100 μL of the resulting solution at a concentration of 100 mg/kg (14) was injected intravenously just before the i.v. injection of the ultrasound contrast agent. Mice were then transferred to the LIPU preclinical platform for sonication. For trafficking and treatment experiments, anti–PD-1, EGFRvIII-CAR T cells, or APCs were delivered i.v. just before i.v. ultrasound contrast agent and sonication. Preclinical studies have shown that for large molecules/therapeutics, the BBB begins closing immediately after sonication, with a theoretical half-closure time of less than 1 hour for molecules larger than 5 nm (15). As such, we delivered the agent just before sonication, when the brain penetration of the agents used would be maximized.

Animals

Mice were housed in the MD Anderson animal facility in accordance with Laboratory Animal Resources Commission standards. Animal experiments were conducted in compliance with the guidelines for animal care and use established by MD Anderson and the federal government. All studies were supervised by the Institutional Animal Care and Use Committee at MD Anderson Cancer Center under protocol 00001544-RN01.

In vivo murine tumor models

To induce intracerebral tumors in C57BL/6 and NSG (The Jackson Laboratory) mice, the GL261 and EGFRvIII-U87 cells were collected in the logarithmic growth phase, loaded into a 25-μL syringe (Hamilton), and injected 2 mm to the right of the bregma and 4 mm below the surface of the skull at the coronal suture using a stereotactic frame (Stoelting). The i.c. tumorigenic doses of GL261 and EGFRvIII-expressing U87 cells were 5.0×10^4 cells and 1.5×10^5 cells, respectively, in total volumes of 2 and 4 μL of PBS, respectively. Mice were randomly assigned to control and treatment groups after tumor implantation. When animals showed signs of neurologic deficit (lethargy, failure to ambulate, lack of feeding, or loss of >20% body weight), they were compassionately killed. These symptoms typically occurred within 48 hours of death.

NanoString gene-expression analysis

C57BL/6 mice were implanted with stereotactic injection of 50,000 GL261 cells as described above. On day 14 after tumor implantation, 10 mice in each group were treated with either PBS or LIPU. On day 16 after tumor implantation, mice were euthanized and brains were

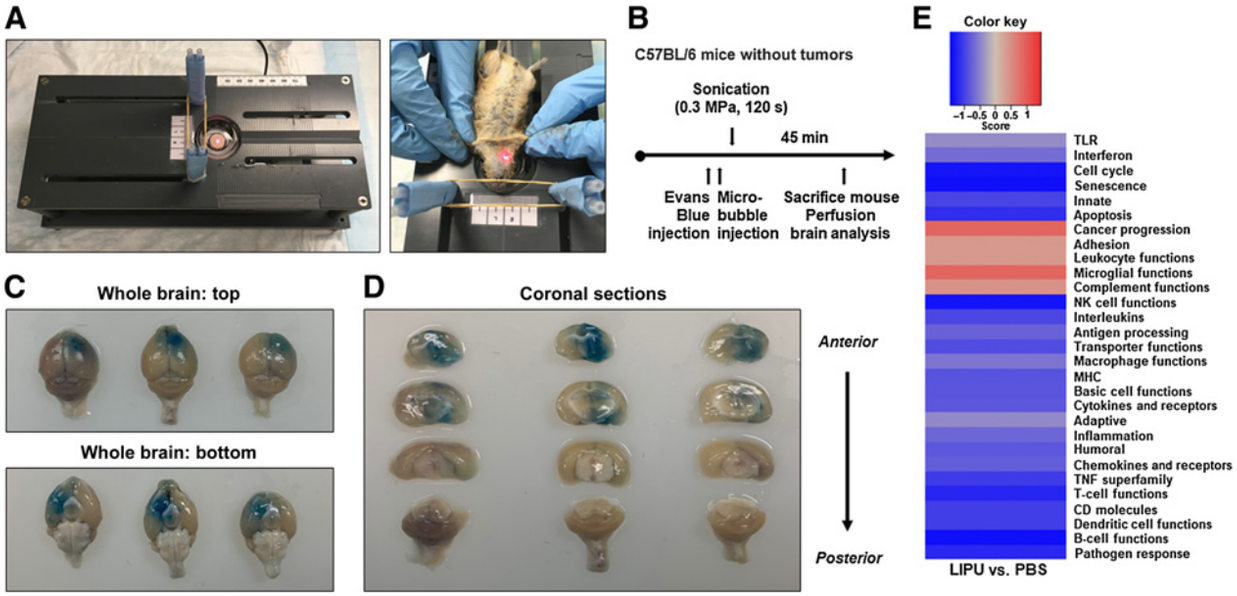

Figure 1.

Ultrasound-mediated BBBD causes reproducible and targeted BBB opening and lacks in immune response modifications. **A,** left, preclinical platform for BBB opening in murine models. Right, the region for BBBD on supine mouse was positioned directly over the ultrasound pulse area using laser guidance (red mark) after the head was secured with elastic bands. **B,** Schema for treatment of non–tumor-bearing C57BL/6 mice with Evans blue dye and ultrasound. Mouse perfusion was followed by gross brain analysis 45 minutes after dye injection. **C,** Representative photographs of whole brains from superior and inferior projections taken immediately after mouse perfusion and brain dissection. **D,** Perfused whole brains coronally sectioned from anterior to posterior (same order from left to right as in **C**). **E,** Directed global significance scores of immune gene sets in the LIPU group compared with the PBS control. Red indicates gene sets with overexpression while blue indicates gene sets with underexpression.

collected after cardiac perfusion with PBS. Percoll density gradient centrifugation was then used for immune cell isolation from the hemisphere of tumor implantation. Immune cells underwent mRNA extraction (RNeasy Plus Mini Kit, Quiagen) for NanoString analysis. Analysis of mRNA was performed with the nCounter PanCancer Immune Profiling Panel (NanoString Technologies, Inc.). Sample preparation and hybridization was performed as described previously (16). Target molecules were quantified by imaging immobilized fluorescent reporters using the nCounter Digital Analyzer. mRNA gene expression of 770 immune-related genes was analyzed using the nSolver 4.0, R version 3.3.2, and Advanced Analysis 2.0 software. The genes specific to functional signaling pathways and immune cell types were categorized based on the attached manual.

Anti–PD-1 fluorescent tagging and *in vivo* biodistribution analysis

The anti–PD-1 antibody (BE0146, clone RMP1-14) was fluorescently tagged with Alexa Fluor 647 using a SAIVI Rapid Ab Labeling Kit (S30044, Invitrogen) according to the manufacturer's recommendations. Briefly, 1 mg of the antibody at a concentration of 2 mg/mL was incubated with the Alexa Fluor 647 dye for 1 hour at room temperature, run through a 3-cm column containing kit resin, and collected as elution fractions. Purified conjugated antibody absorbance was measured at 280 and 650 nm, and protein concentrations were calculated using a NanoDrop 1000 spectrophotometer (Thermo Fisher Scientific).

Treatment with anti–PD-1 monoclonal antibodies

Monoclonal antibodies against PD-1 (BE0146, clone RMP1-14) were obtained from Bio X Cell. Mice were treated with i.v. injections of isotype control IgG (200 μg/mouse; Bio X Cell), the anti–PD-1 antibody (200 μg/mouse; Bio X Cell), or the anti–PD-1 antibody with ultrasound. Treatments were performed on days 3, 7, 10, 14, and 17, or on days 12, 15, and 19 after i.c. tumor implantation. Animals that died prior to the initiation of at least three treatments were not included in the survival analysis.

EGFRvIII-CAR construction

Human CAR T cells were engineered using an EGFRvIII-CAR made by fusing the single-chain variable fragment of the EGFRvIII-specific monoclonal antibody mAB 139. The single-chain variable fragment was attached to an IgG4 stalk and intracellular CD28 and CD3-zeta signaling domains as previously described (17). A shortened *ex vivo* production strategy established in our lab was used to create CAR T cells with an improved immune phenotype associated with greater therapeutic outcomes compared with CAR T cells produced under the current gold-standard protocol of CAR production (17). The CAR plasmid was modified to express a firefly luciferase (ffLuc) bioluminescent reporter for CAR monitoring *in vivo*. Human peripheral blood mononuclear cells from healthy donors underwent negative selection for $CD3^+$ T cells followed by electroporation of the Sleeping Beauty transposon containing CAR with the sleeping beauty transposase SB11. CAR T cells were expanded *in vitro* over 14 days by combining them with irradiated activating and propagating cells, IL2, and IL21. Before murine CAR T-cell administration, CAR expression was quantified using flow cytometry with an anti-Fc antibody to detect the IgG4 portion of the CAR. EGFRvIII/ffLuc CAR T cells (1.5×10^7) were administered intravenously for bioluminescent imaging (BLI) experiments and treatment.

IHC

NSG mouse brains were fixed in 10% formalin for 36 hours followed by 70% ethanol. Brains were then paraffin-embedded with 4-μm sections being used for IHC analysis. IHC staining was carried out according to manufacturer's recommendations listed in the Vectastain ABC Kit (cat. No. PK-4002, Vector Laboratories). An anti-human CD3 antibody (1:50) was purchased from Agilent and (cat. No. M725429-2, Agilent) was used for detection of EGFRvIII-CAR T cells. Microscopic fields imaged at 400× magnification in tumor-bearing brains of mice taken from each group.

CXCL9 and CXCL10 gene transduction into F4/80$^+$CD11c$^+$ antigen-presenting cells

To transduce the CXCL9 and CXCL10 immune chemokine genes into the APCs, we prepared lentiviruses that encoded the cDNA of murine CXCL9 or CXCL10 gene transfer plasmids (cat. No. MR200667L3 and cat. No. MR200291L4, respectively; Origene). Under sterile conditions, bone marrow cells were extracted from 6-week-old female C57BL/6 mice as previously described (18). Red blood cells from the bone marrow were lysed with 0.84% ammonium chloride, and lymphocytes, granulocytes, and Ia$^+$ cells were depleted using Low-Tox-M rabbit complement (Cedarlane) with the following monoclonal antibodies: GK1.5 (CD4), 2.43 (CD8), RA3-3A1/6.1 (CD45R), B21-2 (class II), and RB6-8C5 (Gr-1). Depleted cells were plated in six-well cell culture plates (3×10^6 cells/well) in Roswell Park Memorial Institute medium 1640 supplemented with 5% (vol/vol) fetal bovine serum, 50 mmol/L β-mercaptoethanol, 10 mmol/L Hepes, 2 mmol/L glutamine, 100 U/mL penicillin, 100 mg/mL streptomycin, and 1,000 U/mL granulocyte–macrophage colony-stimulating factor (Immunex) or in AIM-V (Gibco BRL) supplemented with 1,000 U/mL of granulocyte–macrophage colony-stimulating factor. Floating cells were removed on day 3, and on day 7 nonadherent cells were replated. On day 10, nonadherent cells were removed for phenotypic analysis using a FACScan flow cytometer for examination of the surface marker expression of F4/80 and CD11c (19). The cells were infected with 5 mL of a freshly prepared lentivirus (transducing units = $6.5 \times 10e^6$/mL), encoding either CXCL9 or CXCL10. Chemokine production was measured using an ELISA (cat. No. ab203364 and cat. No. ab214563, Abcam) according to the manufacturer's instructions.

Ex vivo flow analysis of tumor-infiltrating immune cells

C57BL/6 mice intracranially implanted with GL261 cells underwent treatment with CXCL10 APC cells as described above. On day 12 after tumor implantation, mice were anesthetized before undergoing euthanasia with cardiac perfusion using 30 mL of PBS followed by tumor-implanted brain hemisphere collection. Percoll gradient density centrifugation was used for immune cell isolation. Cells were stained with the fixable viability dye APC-eFluor780 (Thermo Fisher Scientific) to exclude dead cells. For analysis of immune cell populations, extracellular staining was performed with anti-mouse CD45 BV421 (clone 30-F11), CD3 PerCPcy5.5 (clone 17A2), CD4 BV605 (RM4-5), and CD8 PE (53-6.7). Anti-mouse CD16/CD32 (clone 93) was used for prevention of nonspecific binding of the Fc receptors to the detection antibodies. Cells were then permeabilized and fixed using the Foxp3/Transcription Factor Staining Buffer Set (Thermo Fisher) according to the manufacturer's recommendations. All antibodies were purchased from BioLegend. Cells were analyzed using the FACSCelesta (BD Biosciences), and data analysis was performed with FlowJo software.

Statistical analysis

Kaplan–Meier survival analysis was performed, and differences were compared using a log-rank (Mantel–Cox) test and a one-tailed *t* test for independent samples. Statistics from BLI data were calculated using the *F* test to compare variances, and statistics from *ex vivo* flow cytometry were assessed by the two-sided unpaired *t* test.

Results

LIPU reproducibly opened the BBB in preclinical models

Evans blue lacks penetration into the brain when the BBB is intact. Thus, we assessed feasibility and reproducibility of BBB opening with the LIPU preclinical platform by i.v. injecting Evans blue dye before sonication in C57BL/6 mice without tumors and analyzed color changes in the brain parenchyma (**Fig. 1B**). Images of the superior and inferior whole brains showed dye penetration in the anterolateral brain region targeted by the ultrasound beam (**Fig. 1C**). We then sectioned whole brains coronally, which showed that dye was distributed throughout the depth of the brain, from the superior to the inferior regions and in the anterior part of the right hemisphere (**Fig. 1D**). This confirmed the feasibility of reproducible, targeted BBBD in regions of potential tumor implantation.

LIPU alone did not reprogram the immune response or induce a therapeutic effect

The use of LIPU by itself as a therapeutic strategy has been investigated without therapeutic benefit (6) in both GL261 (20) and U87 (11, 21–25) tumors. We investigated if LIPU sonication had the ability to modify the immune response in the glioma microenvironment. On day 14 after GL261 tumor implantation in C57BL/6 mice, 10 mice per group were treated with either PBS or LIPU. On day 16 following tumor implantation, immune cells were isolated from the hemisphere of tumor implantation, and NanoString analysis was performed to investigate possible alterations in a panel of 770 immune-related genes. Immune gene sets were categorized based on function and a directed global significance score was determined based on the extent to which the genes in a gene set were up or down-regulated. A heat map was generated to directly compare LIPU to the PBS control. We found that the LIPU group compared with the PBS group has minimal influence on most immune functions including T-cell functions, inflammation, adaptive immunity, and interleukins (**Fig. 1E**). To clarify if there was a survival benefit in an immune response model, GL261 mice were treated with LIPU and compared with PBS [median survival (MS) duration: 28 days; MS duration: 33 days, respectively] (Supplementary Figure S1A).

Anti–PD-1 CNS delivery is enhanced with LIPU

We administered anti–PD-1 with and without ultrasound BBBD to determine if this method enhances delivery of antibodies to the brain and their function in glioblastoma treatment. We intravenously administered fluorescently tagged anti–PD-1 with ultrasound followed by a 3-hour waiting period for antibody circulation. (**Fig. 2A**). We found that treatment with anti–PD-1 alone resulted in low levels of antibody infiltration in the cerebellum with minimal, focal delivery enhancement of over the potential site of tumor implantation. When we gave labeled anti–PD-1 with LIPU, there was enhanced and localized delivery to brain parenchyma submitted to the ultrasound beam, which was further enhanced with an additional sonication treatment performed immediately after the initial sonication (**Fig. 2B**).

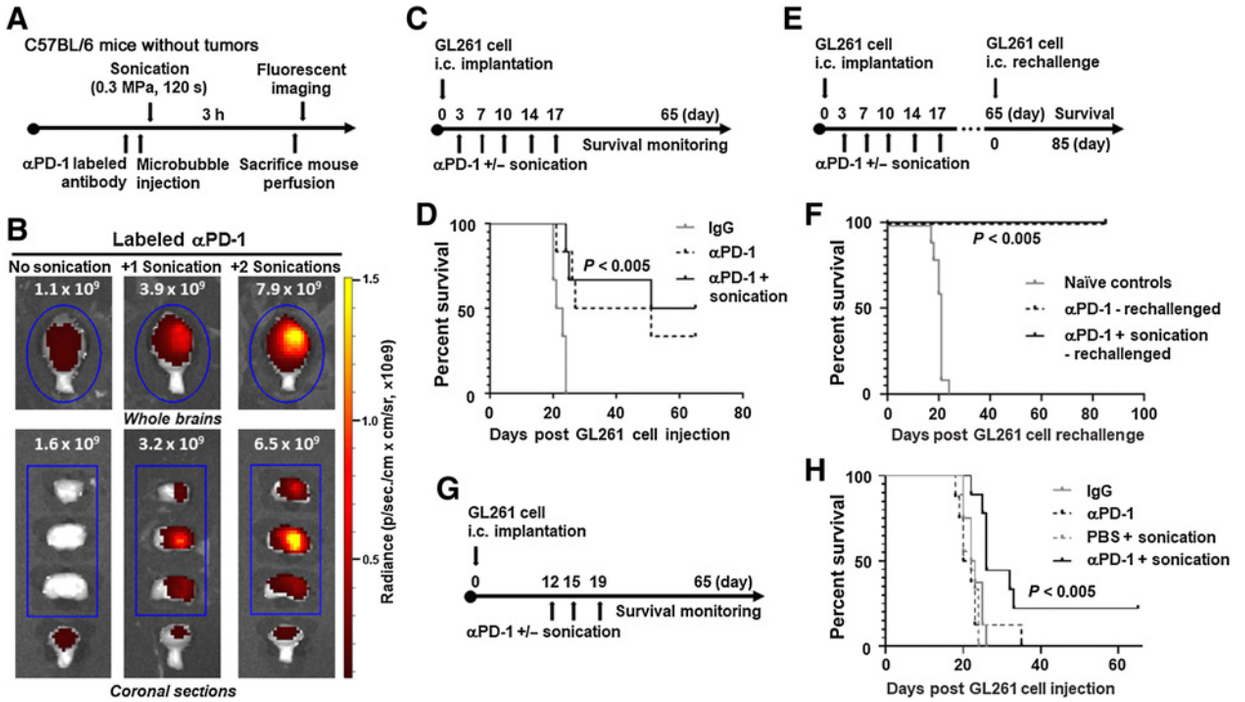

Figure 2.

Anti–PD-1 administered with ultrasound BBBD caused increased delivery of the antibody to the brain and enhanced survival in glioma-bearing mice. **A,** Schema for treatment with labeled anti–PD-1 administered with ultrasound in non–tumor-bearing C57BL/6 mice. **B,** Fluorescent images of whole and coronally sectioned brains performed immediately after perfusion and brain dissection following the treatment described in **A**. Mice were treated with the labeled anti–PD-1 antibody alone (left), labeled anti–PD-1 and one sonication (middle), or labeled anti–PD-1 and two sonications (right). **C,** The treatment schema of GL261 tumor–bearing mice treated with anti–PD-1 with or without LIPU. **D,** Kaplan–Meier survival analysis of C57BL/6 mice treated with IgG (control), anti–PD-1, or anti–PD-1 with ultrasound (six mice per group). PBS with sonication control for the GL261 model is demonstrated in Supplementary Fig. S1A. Survival analysis was performed using the log-rank (Mantel–Cox) test. The MS durations in the treatment groups were as follows: IgG, 22 days; anti–PD-1, 39 days; anti–PD-1 with ultrasound, 58 days. Statistics: IgG versus anti–PD-1, $P = 0.007$; IgG versus anti–PD-1 with ultrasound, $P = 0.0022$; and anti–PD-1 versus anti–PD-1 with ultrasound, $P = 0.6226$. This experiment was repeated with similar findings. **E,** Treatment schema for long-term survivors and naïve age-matched controls which were rechallenged in the contralateral hemisphere. **F,** Kaplan–Meier survival analysis of long-term survivors in **E**. The MS durations in the treatment groups were as follows: naïve controls (10 mice), 21 days; anti–PD-1 (2 mice), undefined; anti–PD-1 with ultrasound (3 mice), undefined. Statistics: naïve control versus anti–PD-1, $P = 0.0148$; naïve control versus anti–PD-1 with ultrasound, $P = 0.0044$. **G,** The treatment schema of GL261 tumor–bearing mice treated with anti–PD-1 with or without LIPU at a later time point when tumors are well established. **H,** Kaplan–Meier survival analysis of C57BL/6 mice treated with IgG (control), anti–PD-1, PBS with ultrasound, or anti–PD-1 with ultrasound (8–9 mice per group). Survival analysis was performed using the log-rank (Mantel–Cox) test. The MS durations in the treatment groups were as follows: IgG, 22.5 days; anti–PD-1, 22 days; PBS with ultrasound, 21 days; anti–PD-1 with ultrasound, 26 days. Statistics: IgG versus anti–PD-1, $P = 0.6186$; IgG versus PBS with ultrasound, $P = 0.1947$; IgG versus anti–PD-1 with ultrasound, $P = 0.0032$; anti–PD-1 versus PBS with ultrasound, $P = 0.7483$; anti–PD-1 versus anti–PD-1 with ultrasound, $P = 0.0164$; and PBS with ultrasound versus anti–PD-1 with ultrasound, $P = 0.0002$.

LIPU further potentiated the impact of anti–PD-1 against CNS gliomas

Although anti–PD-1 antibodies act on peripherally circulating antigen-specific T cells, part of their therapeutic activity is also related to modulation of microglia (26). Because ultrasound enhanced the delivery of anti–PD-1, local modulation of microglia may provide additional therapeutic activity, which we evaluated in glioma-bearing mice. We gave mice bearing established i.c. GL261 tumors twice-weekly i.v. treatments with either IgG, anti–PD-1, or anti–PD-1 immediately prior to ultrasound for 2.5 weeks (**Fig. 2C**). Multiple treatments with anti–PD-1 and ultrasound were safe; we observed no adverse events, behavior changes, or signs of neurologic toxicity. However, repeated dual i.v. treatments led to loss of i.v. access in some mice and, rarely, tail necrosis leading to partial amputation.

The MS duration (58 days) was longer in mice treated with anti–PD-1 and ultrasound than in those treated with IgG (MS duration, 22 days; $P < 0.005$) or anti–PD-1 (MS duration, 39 days; $P = 0.6226$; **Fig. 2D**). Sixty-five days after the initial i.c. implantation, five long-term survivors remained (anti–PD-1, $n = 2$; anti–PD-1 and ultrasound, $n = 3$). We rechallenged these mice along with age-matched naïve controls ($n = 10$) in the contralateral hemisphere to emulate tumor recurrence (**Fig. 2E**). All long-term survivors treated with anti–PD-1 or anti–PD-1 with ultrasound remained alive following rechallenge, whereas all age-matched controls died with an MS duration of 21 days ($P = 0.0148$ and $P < 0.005$, respectively), suggesting an immunologically protective effect (**Fig. 2F**). We then investigated if the significant increase in murine survival in the anti–PD-1 with sonication group would persist if mice were treated at a later time point when tumors were well established. Mice bearing i.c. GL261 tumors were treated with i.v. treatments of either IgG, anti–PD-1, PBS with ultrasound, or anti–PD-1 with ultrasound at days 12, 15, and 17 post tumor implantation (**Fig. 2G**). The MS duration (26 days) was longer in mice treated with anti–PD-1 and ultrasound than in those treated with IgG (MS duration, 22.5 days; $P < 0.005$), anti–PD-1 (MS duration, 21 days; $P < 0.05$), or PBS with ultrasound (MS duration, 22 days; $P > 0.0005$; **Fig. 2H**).

To ascertain if the LIPU strategy could overcome therapeutic resistance to immune-checkpoint inhibitors, C57BL/6 mice were implanted with a murine immunocompetent glioblastoma stem cell line derived from *Nestin-CreER^{T2} Qk$^{L/L}$; Trp53$^{L/L}$; Pten$^{L/L}$* mice (QPP), which served as an immune-checkpoint inhibitor-resistant model. Mice with established i.c. QPP4 tumors were treated twice-weekly i.v. with either PBS, anti–PD-1, PBS prior to ultrasound, or anti–PD-1 prior to ultrasound for 3 weeks (Supplement 1B). Anti–PD-1 and ultrasound (MS duration, 61 days) did not overcome the tumor's resistance to immune-checkpoint inhibitor therapy as no survival benefit was seen compared with mice treated with PBS (MS duration, 81 days), PBS and ultrasound (MS duration, 61 days), or anti–PD-1 (MS duration, 127.5 days; Supplement 1C).

LIPU enhanced CAR T cells' trafficking to the glioma microenvironment

To determine if cellular therapies such as CAR T cells can be improved by increasing the distribution of cells to the tumor microenvironment with LIPU, we directly compared the delivery and persistence of CAR T cells administered with and without BBB opening. We modified the CAR plasmid to express a ffLuc fluorescent reporter for CAR monitoring *in vivo* by BLI. We verified the expression of the CAR and that the T-cell population contained both CD4$^+$ and CD8$^+$ T cells (**Fig. 3A**), which have been shown to generate a superior response (27, 28). We used ffLuc-labeled EGFRvIII-CAR T cells to determine whether ultrasound-mediated BBBD affects cellular therapy trafficking and persistence *in vivo* (**Fig. 3B**). BLI demonstrated that most CARs were distributed to the liver and lungs, making up most of the thoracic signal, with a small fraction distributed to the brain (**Fig. 3C**). In mice administered both EGFRvIII-CAR T cells and sonication, CAR T-cell bioluminescence increased significantly from 24 to 72 hours after treatment ($P < 0.005$ and $P < 0.0001$, respectively; **Fig. 3D**), indicating that LIPU enhances the focal delivery and the persistence of CARs in the brain. Representative IHC staining verified the BLI findings of enriched EGFRvIII-CAR T-cell delivery to the tumor microenvironment with ultrasound out to 15 days after treatment (**Fig. 3E**).

Ultrasound administration of EGFRvIII-CAR T cells increased survival durations in murine glioblastoma models

Because LIPU-induced BBBD increased CAR T-cell trafficking to the tumor and longer persistence when compared with CAR T cells administered alone, we investigated whether this difference could have biologically significant effects *in vivo*. NSG mice bearing EGFRvIII-U87 tumors treated with i.v. EGFRvIII/ffLuc CAR T cells and ultrasound 14 days after tumor implantation (**Fig. 4A**) had an undefined MS duration (>80 days) relative to mice treated with CAR T cells alone (MS duration, 35 days; $P < 0.05$; **Fig. 4B**). Administration of EGFRvIII-

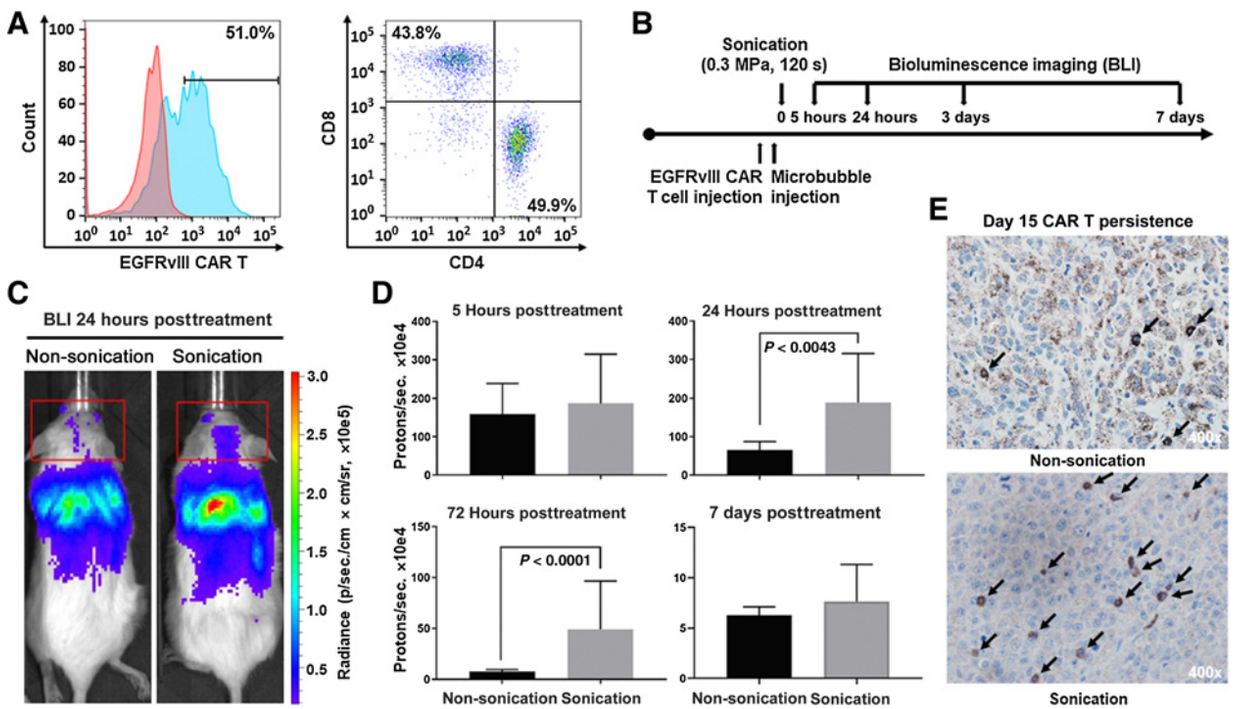

Figure 3.

Intravenously administered CAR T cells treated with ultrasound BBBD increased trafficking of CAR T cells to the brain and persistence of CAR T cells in the tumor microenvironment. **A,** Expression of the EGFRvIII-CAR, and CD4$^+$ and CD8$^+$ T-cell populations were demonstrated by flow cytometry in the lymphocyte population. **B,** Treatment schema for BLI of ffLuc CAR T cells administered intravenously in mice implanted with EGFRvIII-expressing U87 tumors **C**. Representative example of CAR T-cell trafficking from BLI of mice administered CAR T cells intravenously, without (left) and with (right) ultrasound. The red boxes demonstrate BLI measurements of CAR T cells present in the head. **D,** Summary of CAR T-cell BLI signals in the head. Statistics: 24 hours non-ultrasound versus ultrasound, $P = 0.0043$; 72 hours non-ultrasound versus ultrasound, $P < 0.0001$. Statistical analysis was performed using the F test to compare variances. The respective numbers of mice in the non-ultrasound and ultrasound groups were as follows: 5 hours, 5 and 9; 24 hours, 5 and 9; 72 hours, 4 and 9; 7 days, 3 and 9. **E,** IHC of EGFRvIII U87 bearing NSG mice 15 days after treatment with EGFRvIII/ffLuc CAR T cells administered intravenously without ultrasound (top) and with ultrasound (bottom). CAR T cells stained with anti-human CD3 antibody and images shown at 400× magnification.

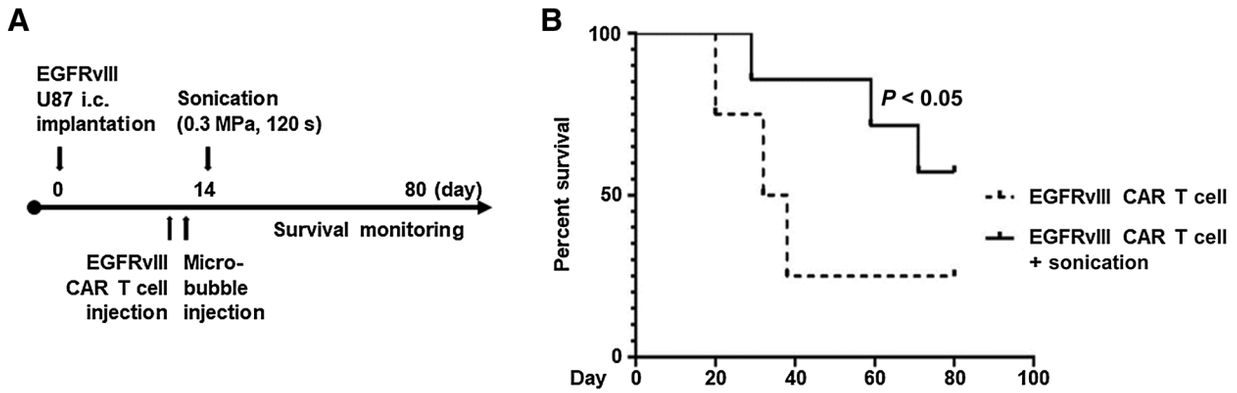

Figure 4.

Ultrasound-mediated BBBD with CAR T-cell therapy was associated with increased mouse survival durations. **A,** Treatment schema for NSG mice bearing EGFRvIII-expressing U87 tumors and treatment on day 14 with EGFRvIII/ffLuc CAR T cells. **B,** Survival of NSG mice treated with EGFRvIII-CAR T cells or EGFRvIII-CAR T cells with ultrasound. Survival was determined using Kaplan–Meier analysis with a one-tailed *t* test for independent samples. The MS duration in the treatment groups were as follows: EGFRvIII-CAR T-cell (four mice), 35 days; EGFRvIII-CAR T cells with ultrasound (seven mice), undefined. Statistics: EGFRvIII-CAR T cells versus EGFRvIII-CAR T cells with ultrasound, $P = 0.04423$.

CAR T cells did lead to mild signs of systemic toxicity in both groups, demonstrated by hunched posture for up to 3 days following treatment. However, mice returned to baseline without long-term adverse effects or signs of neurologic toxicity.

APCs producing the T-cell attracting chemokine CXCL10 were efficacious when combined with LIPU

Our studies using CAR T cells demonstrated that ultrasound can enhance the administration of cellular immunotherapies. Based on the paucity of APCs within the tumor microenvironment (4), we hypothesized that an APC could be modified to express a T-cell attracting chemokine that could enhance localized immune activation and that LIPU-induced BBBD would enhance delivery of these APCs at the site of tumor antigens. Accordingly, we isolated murine APCs from the bone marrow of C57BL/6 mice and modified them via lentiviral transduction to encode the cDNA of CXCL9 or CXCL10 (**Fig. 5A**; ref. 29) or methionine-deficient green fluorescent protein (control) for cell tagging (**Fig. 5B**). We used flow cytometry for phenotypic analysis of APCs for F4/80 and CD11c surface markers and an ELISA to analyze chemokine production of CXCL9 or CXCL10 (3,392 pg/mL and 2,987 pg/mL, respectively, with stable transduction even after APC storage at −80°C).

We examined if CXCL10 expressing APCs had the capacity to alter the tumor microenvironment by increasing the frequency of T cells. C57BL/6 mice were treated with 1×10^6 CXCL10 APCs with and without LIPU on day 7 and mice were terminated on day 12 following tumor implantation. Day 12 was selected for immune cell analysis in the therapeutic window in order to ensure tumors were large enough to analyze, but not at a point of treatment failure. Immune cells were isolated from the tumor implanted hemisphere of all treatment groups and analyzed by multicolor flow cytometry. Live single $CD45^+$ immune cells were gated on $CD3^+$, $CD4^+$, and $CD8^+$ expression, and the percentage of T cells within the total number of $CD45^+$ cells was calculated (Supplementary Fig. S1D). LIPU administration of CXCL10 APCs significantly increased the percentage of $CD3^+$ (**Fig. 5C**), $CD4^+$ (**Fig. 5D**) T cells relative to all other treatment groups, and $CD8^+$ T cells relative to control PBS with LIPU (**Fig. 5E**) in the glioma microenvironment.

To ascertain whether ultrasound administration of CXCL9 or CXCL10 APCs was therapeutically effective, we implanted C57BL/6 mice with GL261 cells and gave them 1×10^6 CXCL9 or CXCL10 overexpressing APCs intracranially or intravenously with or without ultrasound (**Fig. 5F**). Mice tolerated the treatments well without any adverse events, behavior changes, or neurologic toxicity. Survival analysis of mice treated with CXCL9 expressing APCs using i.c., or i.v. with and without LIPU, showed no significant survival benefit compared with PBS-treated control mice (Supplementary Fig. S1E). However, in mice treated with CXCL10-expressing APCs, those that underwent i.c. administration had significantly better survival durations than did the PBS control group, demonstrating the cellular therapy was effective when administered directly to the tumor microenvironment ($P < 0.05$). Mice treated with i.v. administration of the same concentration of CXCL10 APCs had no survival benefit over those in the PBS group ($P = 0.6041$). When we gave this cellular therapy intravenously with LIPU, we found there was a significantly better survival duration than in the PBS ($P < 0.05$), i.v.-only ($P < 0.05$), and i.c.-only ($P < 0.05$) groups (**Fig. 5G**).

Discussion

LIPU is a promising technique that allows for transient BBBD (8). The safety of the technique has been largely studied including microscopic, macroscopic, and clinical analysis of tissues in small and large preclinical animal models (12, 30–33) and more recently in human clinical trials (34–38). The data included in our study explore the potential of LIPU for enhancing the therapeutic efficacy of immunotherapy in preclinical models. This technique of disrupting the BBB using ultrasound is now being studied in eight ongoing clinical trials with both implantable and transcranial focused ultrasound devices (NCT04446416, NCT04614493, NCT04528680, NCT03744026, NCT04063514, NCT03551249, NCT03616860, and NCT03712293). The immunotherapy approaches proposed herein could thus be rapidly explored using these clinical-stage devices in trials to further examine their potential for treatment of glioblastoma. NanoString analysis of gene sets comprised of 770 immune-related genes indicated LIPU sonication alone may not prime the immune response in a manner necessary for a survival advantage. This suggests that an

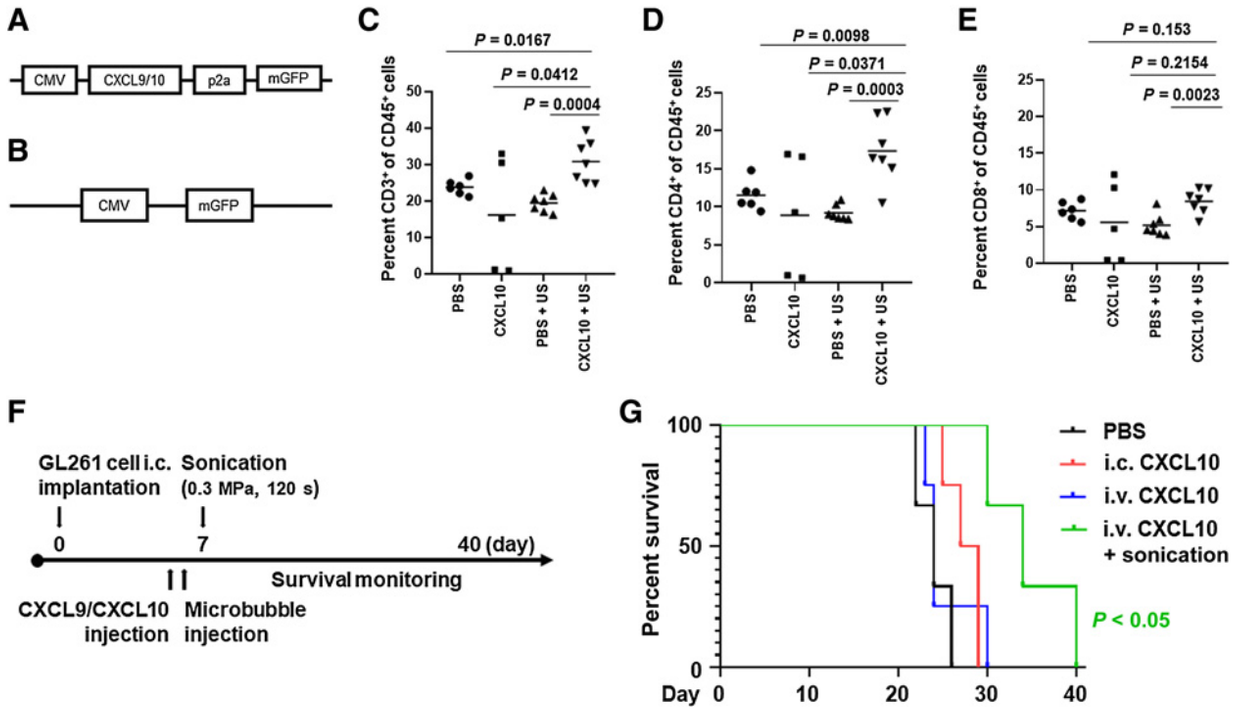

Figure 5.

APCs expressing CXCL10 administered intravenously with LIPU-induced BBBD were associated with a significant increase in immunocompetent mouse survival durations. **A,** Schema of the lentivirus gene transfer plasmid structure for murine CXCL9 or CXCL10. **B,** Gene transfer plasmid of control methionine-deficient green fluorescent protein alone. **C,** Flow cytometry analysis of the percentage of $CD3^+$ T cells within the total $CD45^+$ immune cell infiltration within intracerebral gliomas in the different treatment groups ($n = 5$–7/group). Statistics: PBS versus CXCL10 with ultrasound, $P = 0.0167$; CXCL10 versus CXCL10 with ultrasound, $P = 0.0412$; PBS with ultrasound versus CXCL10 with ultrasound, $P = 0.0004$. **D,** Flow cytometry analysis of $CD4^+$ T cells within the total $CD45^+$ immune cell infiltration within intracerebral gliomas. Statistics: PBS versus CXCL10 with ultrasound, $P = 0.0098$; CXCL10 versus CXCL10 with ultrasound, $P = 0.0371$; PBS with ultrasound versus CXCL10 with ultrasound, $P = 0.0003$. **E,** Flow cytometry analysis of $CD8^+$ T cells within the total $CD45^+$ immune cell infiltration within intracerebral gliomas. Statistics: PBS with ultrasound versus CXCL10 with ultrasound, $P = 0.0023$; PBS versus CXCL10 with ultrasound, $P = 0.153$; CXCL10 versus CXCL10 with ultrasound, $P = 0.2154$, as assessed by the two-sided unpaired *t* test. **F,** Treatment schema for C57BL/6 mice bearing GL261 tumors treated with CXCL9 or CXCL10 APCs. **G,** Kaplan–Meier survival analysis of mice treated with PBS, i.c. CXCL10 APCs, i.v. CXCL10 APCs, or i.v. CXCL10 APCs with ultrasound. PBS with sonication control for the GL261 model is demonstrated in Supplementary Fig. S1A. The MS durations in the treatment groups were as follows: PBS (3 mice), 24 days; i.c. CXCL10 APCs (4 mice), 28 days; i.v. CXCL10 APCs (4 mice), 24 days; i.v. CXCL10 APCs with ultrasound (3 mice), 34 days. Statistics: PBS versus i.c. CXCL10 APCs, $P = 0.0476$; PBS versus i.v. CXCL10 APCs, $P = 0.6041$; PBS versus i.v. CXCL10 APCs with ultrasound, $P = 0.0246$; i.c. CXCL10 APCs versus i.v. CXCL10 APCs, $P = 0.6349$; i.c. CXCL10 APCs versus i.v. CXCL10 APCs with ultrasound, $P = 0.0213$; i.v. CXCL10 APCs versus i.v. CXCL10 APCs with ultrasound, $P = 0.0415$.

immunotherapy would be necessary in combination with LIPU BBBD for modification of the tumor microenvironment and improved survival. We cannot, however, exclude the possibility that further modifications of the LIPU conditions such as increasing the mechanical index or the amount of microbubbles could trigger an antitumor immune response. Moreover, a wide panel of therapeutic agents has been delivered to the brain in preclinical models including small molecular-weight molecules (20, 39), antibodies (9, 22), or cells (7, 40). Thus, LIPU-induced BBBD could increase the presence of desirable immune cells such as $CD8^+$ cytotoxic T cells (adoptive T cells, CARs, etc.), which are normally scarce in the tumor microenvironment. However, this technique must be specific enough to limit undesirable tumor-supportive and immunosuppressive cells such as regulatory T cells, M2 macrophages, and myeloid-derived suppressors. Accordingly, in our study, we focused on the delivery of specific immune-cell subtypes and immunomodulators that would favorably tip the balance toward proinflammatory responses rather than just lead to a generalized increase in the number of overall immune cells.

Of the strategies we tested, the use of anti–PD-1 is the most immediate, globally available strategy that could be implemented in clinical trials. Adding LIPU improved anti–PD-1 delivery and was protective to tumor rechallenge. Previous studies demonstrated immune-checkpoint inhibitor-mediated immune memory responses (41–44). Treatment of GL261 tumors at day 12 shows similarities to phase III clinical trials where anti–PD-1 alone fails to improve overall survival for glioblastoma. Treatment with anti–PD-1 and sonication at the later time point does provide an increase in murine survival. By enhancing both T-cell and anti–PD-1 delivery across the BBB with ultrasound, $CD4^+$ and $CD8^+$ T-cell dysfunction in the tumor microenvironment may be prevented, thereby allowing for greater effector responses (**Fig. 6A**). Notably, the use of LIPU-induced BBBD with anti–PD-1 would still require an enrichment biomarker of response for human clinical trials because the use of this therapeutic modality will not likely overcome therapeutic resistance as was shown with the QPP4 glioma model. LIPU-induced BBBD did enhance the *in vivo* persistence in the tumor microenvironment of CAR T cells that correlated with increased survival, likely secondary to CAR-mediated recognition of tumor antigens and increased tumor-cell killing (**Fig. 6B**). Significant increases in BLI signal at 24 and 72 hours in the brains of LIPU administered CAR T-cell mice are

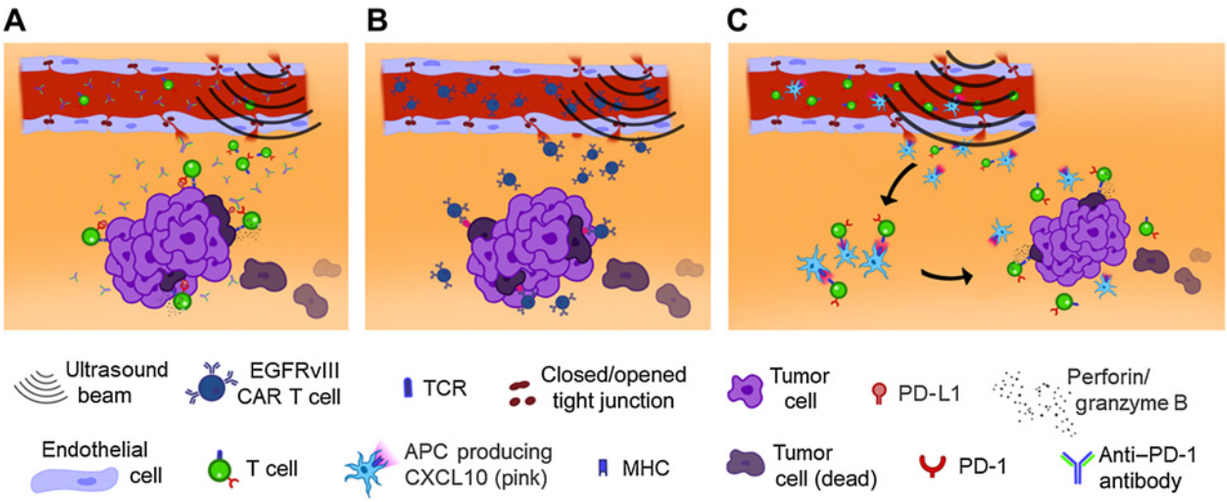

Figure 6.

Schemas demonstrating how ultrasound-mediated BBBD delivers antibodies, CAR T cells, and APCs to the tumor microenvironment for immune activation and improved tumor-cell killing. **A,** Anti–PD-1 delivered through an open BBB blocks immune exhaustion of effector T cells, thereby enabling T cells to exert an effector response through perforin and/or granzyme B. **B,** Compared with CAR T cells administered alone, ultrasound-administered CAR T cells can infiltrate the tumor microenvironment more diffusely and with longer persistence, thereby triggering tumor cytotoxicity through the CARs. **C,** Ultrasound BBB opening allows CXCL10 APCs and T cells to infiltrate the tumor microenvironment. Secondary to the APC presenting antigens to the T-cell, the T-cell becomes activated and thus can mediate direct tumor killing because the T cells have not been chronically stimulated.

outside the 4- to 8-hour window of transient BBB opening. As such, a nonsignificant increase in the CAR T cells during the first hours may result in an increased persistence or a significant expansion after BBB closure secondary to recognition of tumor antigens. Alternatively, the LIPU-induced BBBD may enhance antigen availability, thereby enhancing CAR persistence. CAR T-cell administration with LIPU may enhance distribution and persistence in the glioma microenvironment, which can be administered repeatedly for amplified immune responses.

The current dogma is that anti-glioma immune responses are generated by the lymphatic drainage of antigens into the cervical lymph nodes (45), where APCs like dendritic cells present antigens to T cells, which then trigger T-cell cytotoxic effector functions (46). These T cells then traffic to the local tumor microenvironment to eradicate the glioma. However, immune phenotyping reveals that these T cells lack effector function and are exhausted (47). Chronic T-cell stimulation with weak tumor antigens will precipitate this state (48). The T-cell receptor repertoire differs in lymph nodes and the primary cancer (49) and even within various regions of the malignancy itself (50), indicating differences in antigen profiles in various anatomic locations. To date, matched antigenic profiling between tumors and lymph nodes has yet to be conducted, but based on T-cell receptor repertoire analysis, antigenic differences are plausible. During the initial antigen-presentation event, immune checkpoints are not yet significantly upregulated or exhausted (51). Thus, T cells can exert effector responses, including eradication of the tumor. If the glioma microenvironment has sufficient APCs capable of presenting novel antigens to a naïve T cell, then these cells could induce antitumor effector responses.

In nanostring profiling of primary gliomas and brain metastases, we noted marked differences in the frequency of activated dendritic cells in the CNS tumor microenvironment, with these cells (i.e., APCs) being almost completely absent in high-grade gliomas (52). Furthermore, we found that marked dendritic cell and T-cell cluster interactions can be induced in preclinical glioma models using radiation plus a STAT3 inhibitor to maintain dendritic cell activation (16, 53). Therefore, we evaluated the use of LIPU-induced BBBD to deposit APCs into the tumor microenvironment in a uniform, consistent manner. Ultrasound-mediated deposition of CXCL10-expressing APCs loads the tumor microenvironment with T cells that become activated and directed for killing tumor cells (**Fig. 6C**). We found that delivery of the CXCL10-secreting APCs to the glioma microenvironment with LIPU-induced BBBD was superior to delivery with direct i.c. injection. This may have been because of more diffuse dispersal of the APCs throughout the tumor microenvironment relative to the direct injection which may have been more focal. Alternatively, APC passage through the perivascular region after LIPU-induced BBBD may have positioned these cells in close proximity to the T cells emigrating from the vascular space into the localized glioma microenvironment. *Ex vivo* flow cytometry demonstrated a significant increase in the frequency of T cells within the glioma microenvironment after CXCL10-secreting APC treatment. The robust $CD4^+$ T-cell infiltration may decrease the threshold for tumor immune recognition by $CD8^+$ T cells by increasing epitope spreading to antigens (54). We also observed that APCs secreting CXCL10 lead to substantial survival benefits in glioma-bearing mice despite not yet being fully optimized for dose, schedule, or blockade of inactivation by an immunosuppressive tumor. The role of CXCL10 in the immunologic effect of DC-based therapies in GL261 glioma–bearing mice has previously been demonstrated. CXCL10 produced by type 1 polarizing DCs play a role in the induction of antigen-specific cytotoxic lymphocytes in C57BL/6 mice, resulting in increased survival in GL261 glioma-bearing mice (55). The association of intratumoral IP-10 plasmid producing CXCL10 and subcutaneously GL261 lysate-pulsed DCs results in reduction of tumor vasculature, necrosis and apoptosis, and immune response, leading to decreased tumor burden and increased survival (56). Based on the minimal effect of anti-CXCL9 in disease severity, Zhu and colleagues suggested that among CXCR3 ligands, CXCL10 plays a predominant

role in recruiting type 1 "antigen-experienced" T cells into the CNS (57). We suspect CXCL10 but not CXCL9 had an impact because the former induces recruitment of microglia (58), $CD8^+$ and $CD4^+$ effector cells (59), and polarizes T cells toward TH1 differentiation (60). Although CXCL9 and CXCL10 both serve as ligands of CXCR3, they may affect different signaling cascades, thus causing diverse effects on T-cell polarization (59). A previous study demonstrated the efficacy of CXCL10-Ig in reducing myeloma development via the recruitment of CD4, CD8, and NK cells (61). Another study found administration of a dipeptidyl peptidase 4 inhibitor suppressed melanoma by increased endogenous levels of CXCL10 (62). Future studies should verify the presence of an immune synapse in the glioma microenvironment with multiplex IHC, T-cell subset analysis, and immune and function phenotyping associated with this local interaction. Besides optimization of the dose and schedule, APC genetic modification is needed to prevent APC immunosuppression and downregulation of major histocompatibility complexes and costimulatory molecules.

Overall, our data demonstrate that LIPU enhances the therapeutic index for a wide variety of immunotherapy strategies for patients with CNS tumors. LIPU may enhance the delivery of immune therapeutics based on *in vivo* bioluminescent imaging or modify the local tumor microenvironment to be more conducive to immune therapeutic clearance. Further studies are needed in the future to confirm the optimal order of sonication and drug administration for a given therapy. Additionally, a key issue with preclinical studies is that they may overrepresent or underrepresent the impact in actual clinical studies. In preclinical models, BBBD, as demonstrated by the Evans blue dye distribution in the present study, covers almost the entire hemisphere, whereas in an actual patient, BBBD is very likely to cover much less (35). The preclinical system used in these studies is based on the SonoCloud implantable ultrasound device (CarThera). The first-generation device, SonoCloud-1, demonstrated safety in recurrent glioblastoma patients and reproducible BBB opening (34, 35). The SonoCloud-1 creates a 1-cm diameter cylindrical volume of BBB disruption that extends to a depth of approximately 6 cm. The next-generation device, SonoCloud-9, is an implanted device that covers a volume of $6 \times 6 \times 6$ cm^3. Several current clinical trials (NCT03744026, NCT04614493, and NCT04528680) are now exploring the use of the SonoCloud-9 to broaden the volume of BBB disruption to the tumor and surrounding infiltrative regions. Although transcranial focused ultrasound usually is associated with smaller volumes, teams are investigating the sonication of larger volumes as well (63, 64). Nonetheless, given the diffuse nature of infiltration in the context of gliomatosis cerebri and/or multifocal glioblastoma, LIPU may still have volume limitations. Preclinical (65, 66) and clinical (67) studies have shown the ability of LIPU to increase circulating brain-derived biomarkers, confirming the technique may allow for liquid biopsy. By inducing the release of tumor antigens, LIPU-induced BBBD could also facilitate activation of peripheral immune cells, thus increasing the immune response induced by BBBD and overcoming the present volume limitations.

There are a number of LIPU parameters that will need to be considered and optimized not only in preclinical models but also during clinical trials that could affect the therapeutic results. These include the time of administration of the therapeutic relative to the sonication, the amount and type of microbubbles administered, the mechanical index and duration of the sonication, acoustic pressure, and the extent of the tumor vasculature (68–70). Even if some of these parameters are optimized in preclinical studies, they may need to be further evaluated and refined in human subjects given the fundamental differences between the preclinical models and the human tumors on size, molecular and immunologic heterogeneity, infiltration of adjacent brain, presence of necrosis, and vasculature. Although current clinical trials focus on achieving greater tumor concentrations of chemotherapy, the use of LIPU with immunotherapy in the setting of glioma patients is now being actively considered. The challenges of evaluating and monitoring immunotherapy in glioma patients will also be the case for their combination with LIPU but does provide further justification for the use of imaging tagged adoptive cellular therapies (71–75). Immune functional assessment and distribution could be done in the context of window-of-opportunity studies (76, 77). In future clinical trials, further studies are needed to confirm the optimal order of sonication and drug administration for a given therapy.

Our preclinical data may underestimate the impact of using anti–PD-1 with LIPU-induced BBBD because these tumors are small and the anti–PD-1 can penetrate into these tumors via the leaky blood–tumor barrier, without the use of LIPU-induced BBBD (26). Although therapeutic activity of anti–PD-1 can be exerted through modulation of local microglia, the primary mechanism of anti–PD-1 may still be through its function on peripheral immune cells. This may account for the more impressive effects on murine survival with cellular therapies and LIPU relative to an immune-checkpoint inhibitor and LIPU. Although the use of BBB opening ultrasound demonstrated the most compelling biological response with EGFRvIII CARs, this strategy would still not overcome the key limitation of antigen loss (78, 79). Ultimately, the clinical relevance of the preclinical model and ultrasound administration platform will only be validated through the implementation of clinical trials.

Authors' Disclosures

K. Beccaria reports a patent for Apparatus for the treatment of brain affections and method implementing thereof issued. H. Caruso reports personal fees from Intrexon Corporation and Ziopharm Oncology during the conduct of the study; personal fees from Intrexon Corporation and Ziopharm Oncology outside the submitted work; in addition, H. Caruso has a patent for US20170158749A1 pending to Intrexon Corporation and Ziopharm Oncology. J.F. de Groot reports grants from CarThera, HaiHe Pharma, and Taiho Pharma, other support from Ziopharm Oncology, WuXi Biologics, and Gilead, personal fees from Del Mar Pharmaceuticals (BC) Ltd, Samus Therapeutics, Inc., Insightec, Bioasis Technologies, Inc., Magnolia Innovation, LLC, Monteris Medical Corporation, Karyopharm Therapeutics Inc., Mundipharma Research Limited, Prelude Therapeutics, Kiyatec, Cure Brain Cancer Foundation, Merck Sharp & Dohme Co., Sapience Therapeutics, GlaxoSmithKline LLC (GSK), ResTORbio, Inc., Roche, GenomiCare, Tocagen, Voyager Therapeutics, Angios, AbbVie, Kairos Venture Investments, Deciphera Pharmaceuticals, Taiho Pharmaceutical Company, Inc., Janssen Global Services, Novartis, Debiopharm Therapeutics, Inc., Novella Clinical, and Blue Earth Diagnostics outside the submitted work; and spouse employed by Ziopharm Oncology; participated in DSMB: VBI Vaccines, Inc [Glioblastoma (VBI-1901)]. M.A. Curran reports grants and personal fees from ImmunoGenesis, Inc., and ImmunoMet, personal fees from Agenus, Inc., Alligator Bioscience, Inc., ImmunOs, Inc., Oncoresponse, Inc., Pieris, Inc., Nurix, Inc., Aptevo, Inc., Servier, Inc., Kineta, Inc., Salarius, Inc., Xencor, Inc., and Amunix, Inc. outside the submitted work; in addition, M.A. Curran has a patent for Methods and Composition for Localized Secretion of anti–CTLA-4 antibodies issued to multiple licensees and a patent for dual specificity antibodies that bind both PD-L1 and PD-L2 and prevent their binding to PD-1 pending to ImmunoGenesis, Inc. C. Desseaux reports other support from CarThera outside the submitted work. M. Canney reports other support from CarThera during the conduct of the study; in addition, M. Canney has a patent submitted pending. A. Carpentier reports personal fees from CarThera outside the submitted work; in addition, A. Carpentier has a patent for SonoCloud issued and licensed to To CarThera. A.B. Heimberger reports nonfinancial support from CarThera during the conduct of the study; other support from Caris Life Sciences, WCG Oncology Advisory Board (Western IRB), Moleculin, DNAtrix, and Celldex Therapeutics, and grants from Codiak Life Sciences and Celularity outside the submitted work; in addition, A.B. Heimberger has a patent for genetically

modified antigen-presenting cells delivered to the glioma microenvironment pending to N/A. No disclosures were reported by the other authors.

Authors' Contributions

A. Sabbagh: Conceptualization, resources, data curation, formal analysis, validation, investigation, methodology, writing–original draft, writing–review and editing. **K. Beccaria:** Conceptualization, resources, data curation, formal analysis, validation, investigation, methodology, writing–original draft, writing–review and editing. **X. Ling:** Data curation, writing–review and editing. **A. Marisetty:** Data curation, writing–review and editing. **M. Ott:** Data curation, writing–review and editing. **H. Caruso:** Data curation, writing–review and editing. **E. Barton:** Data curation, writing–review and editing. **L.-Y. Kong:** Data curation, writing–review and editing. **D. Fang:** Data curation, writing–review and editing. **K. Latha:** Data curation, writing–review and editing. **D.Y. Zhang:** Data curation, writing–review and editing. **J. Wei:** Data curation, writing–review and editing. **J. DeGroot:** Data curation, writing–review and editing. **M.A. Curran:** Data curation, writing–review and editing. **G. Rao:** Data curation, writing–review and editing. **J. Hu:** Data curation, writing–review and editing. **C. Desseaux:** Data curation, writing–review and editing. **G. Bouchoux:** Data curation, writing–review and editing. **M. Canney:** Data curation, writing–review and editing. **A. Carpentier:** Data curation, writing–review and editing. **A.B. Heimberger:** Conceptualization, resources, data curation, formal analysis, supervision, funding acquisition, writing–original draft, project administration, writing–review and editing.

Acknowledgments

The authors acknowledge graphic designer Quentin Beccaria for his help in creating **Fig. 6**, as well as Laura Russell, ELS and Audria Patrick for editorial and administrative support. Funding was provided by the ReMission Alliance Against Brain Tumors, Traver Walsh Foundation, the Anne C. Brooks and Anthony D. Bullock Foundation, the MD Anderson Cancer Center Provost Fund, and NIH/NCI P30CA016672. Funding was not provided by CarThera for this study.

The costs of publication of this article were defrayed in part by the payment of page charges. This article must therefore be hereby marked *advertisement* in accordance with 18 U.S.C. Section 1734 solely to indicate this fact.

Received October 16, 2020; revised March 15, 2021; accepted May 19, 2021; published first May 24, 2021.

References

1. Beccaria K, Sabbagh A, de Groot J, Canney M, Carpentier A, Heimberger AB. Blood-brain barrier opening with low intensity pulsed ultrasound for immune modulation and immune therapeutic delivery to CNS tumors. J Neurooncol 2020;151:65–73.
2. Ledford H. Engineered antibodies cross blood–brain barrier. Nature 2011. Available from: https://doi.org/10.1038/news.2011.319.
3. Wei J, Marisetty A, Schrand B, Gabrusiewicz K, Hashimoto Y, Ott M, et al. Osteopontin mediates glioblastoma-associated macrophage infiltration and is a potential therapeutic target. J Clin Invest 2019;129:137–49.
4. Wang Q, Hu B, Hu X, Kim H, Squatrito M, Scarpace L, et al. Tumor evolution of glioma-intrinsic gene expression subtypes associates with immunological changes in the microenvironment. Cancer Cell 2017;32:42–56.e6.
5. Hussain SF, Yang D, Suki D, Aldape K, Grimm E, Heimberger AB. The role of human glioma-infiltrating microglia/macrophages in mediating antitumor immune responses. Neuro Oncol 2006;8:261–79.
6. Chongsathidkiet P, Jackson C, Koyama S, Loebel F, Cui X, Farber SH, et al. Sequestration of T cells in bone marrow in the setting of glioblastoma and other intracranial tumors. Nat Med 2018;24:1459–68.
7. Alkins R, Burgess A, Kerbel R, Wels WS, Hynynen K. Early treatment of HER2-amplified brain tumors with targeted NK-92 cells and focused ultrasound improves survival. Neuro Oncol 2016;18:974–81.
8. Hynynen K, McDannold N, Vykhodtseva N, Jolesz FA. Noninvasive MR imaging-guided focal opening of the blood-brain barrier in rabbits. Radiology 2001;220:640–6.
9. Kinoshita M, McDannold N, Jolesz FA, Hynynen K. Noninvasive localized delivery of Herceptin to the mouse brain by MRI-guided focused ultrasound-induced blood-brain barrier disruption. Proc Natl Acad Sci U S A 2006;103:11719–23.
10. Shingu T, Ho AL, Yuan L, Zhou X, Dai C, Zheng S, et al. Qki deficiency maintains stemness of glioma stem cells in suboptimal environment by downregulating endolysosomal degradation. Nat Genet 2017;49:75–86.
11. Dréan A, Lemaire N, Bouchoux G, Goldwirt L, Canney M, Goli L, et al. Temporary blood-brain barrier disruption by low intensity pulsed ultrasound increases carboplatin delivery and efficacy in preclinical models of glioblastoma. J Neurooncol 2019;144:33–41.
12. Beccaria K, Canney M, Goldwirt L, Fernandez C, Adam C, Piquet J, et al. Opening of the blood-brain barrier with an unfocused ultrasound device in rabbits. J Neurosurg 2013;119:887–98.
13. Uyama O, Okamura N, Yanase M, Narita M, Kawabata K, Sugita M. Quantitative evaluation of vascular permeability in the gerbil brain after transient ischemia using Evans blue fluorescence. J Cereb Blood Flow Metab 1988;8:282–4.
14. Wang F, Cheng Y, Mei J, Song Y, Yang YQ, Liu Y, et al. Focused ultrasound microbubble destruction-mediated changes in blood-brain barrier permeability assessed by contrast-enhanced magnetic resonance imaging. J Ultrasound Med 2009;28:1501–9.
15. Marty B, Larrat B, Van Landeghem M, Robic C, Robert P, Port M, et al. Dynamic study of blood-brain barrier closure after its disruption using ultrasound: a quantitative analysis. J Cereb Blood Flow Metab 2012;32:1948–58.
16. Ott M, Kassab C, Marisetty A, Hashimoto Y, Wei J, Zamler D, et al. Radiation with STAT3 blockade triggers dendritic cell-T cell interactions in the glioma microenvironment and therapeutic efficacy. Clin Cancer Res 2020;26:4983–94.
17. Caruso HG, Tanaka R, Liang J, Ling X, Sabbagh A, Henry VK, et al. Shortened ex vivo manufacturing time of EGFRvIII-specific chimeric antigen receptor (CAR) T cells reduces immune exhaustion and enhances antiglioma therapeutic function. J Neurooncol 2019;145:429–39.
18. Heimberger AB, Crotty LE, Archer GE, McLendon RE, Friedman A, Dranoff G, et al. Bone marrow-derived dendritic cells pulsed with tumor homogenate induce immunity against syngeneic intracerebral glioma. J Neuroimmunol 2000;103:16–25.
19. Sheng J, Chen Q, Soncin I, Ng SL, Karjalainen K, Ruedl C. A Discrete subset of monocyte-derived cells among typical conventional type 2 dendritic cells can efficiently cross-present. Cell Rep 2017;21:1203–14.
20. Kovacs Z, Werner B, Rassi A, Sass JO, Martin-Fiori E, Bernasconi M. Prolonged survival upon ultrasound-enhanced doxorubicin delivery in two syngenic glioblastoma mouse models. J Control Release 2014;187:74–82.
21. Shen Y, Pi Z, Yan F, Yeh CK, Zeng X, Diao X, et al. Enhanced delivery of paclitaxel liposomes using focused ultrasound with microbubbles for treating nude mice bearing intracranial glioblastoma xenografts. Int J Nanomedicine 2017;12:5613–29.
22. Liu HL, Hsu PH, Lin CY, Huang CW, Chai WY, Chu PC, et al. Focused ultrasound enhances central nervous system delivery of bevacizumab for malignant glioma treatment. Radiology 2016;281:99–108.
23. Deibert CP, Zussman BM, Engh JA. Focused ultrasound with microbubbles increases temozolomide delivery in U87 transfected mice. Neurosurgery 2015;76:N22–3.
24. Wu M, Chen W, Chen Y, Zhang H, Liu C, Deng Z, et al. Focused ultrasound-augmented delivery of biodegradable multifunctional nanoplatforms for imaging-guided brain tumor treatment. Adv Sci 2018;5:1700474.
25. Liu HL, Huang CY, Chen JY, Wang HY, Chen PY, Wei KC. Pharmacodynamic and therapeutic investigation of focused ultrasound-induced blood-brain barrier opening for enhanced temozolomide delivery in glioma treatment. PLoS One 2014;9:e114311.
26. Rao G, Latha K, Ott M, Sabbagh A, Marisetty A, Ling X, et al. Anti-PD-1 Induces M1 polarization in the glioma microenvironment and exerts therapeutic efficacy in the absence of CD8 cytotoxic T cells. Clin Cancer Res 2020;26:4699–712.
27. Sommermeyer D, Hudecek M, Kosasih PL, Gogishvili T, Maloney DG, Turtle CJ, et al. Chimeric antigen receptor-modified T cells derived from defined CD8+ and CD4+ subsets confer superior antitumor reactivity in vivo. Leukemia 2016;30:492–500.

28. Turtle CJ, Hanafi LA, Berger C, Gooley TA, Cherian S, Hudecek M, et al. CD19 CAR-T cells of defined CD4+:CD8+ composition in adult B cell ALL patients. J Clin Invest 2016;126:2123–38.
29. van der Woude LL, Gorris MAJ, Halilovic A, Figdor CG, de Vries IJM. Migrating into the tumor: a roadmap for T cells. Trends Cancer 2017;3:797–808.
30. Tung YS, Marquet F, Teichert T, Ferrera V, Konofagou EE. Feasibility of noninvasive cavitation-guided blood-brain barrier opening using focused ultrasound and microbubbles in nonhuman primates. Appl Phys Lett 2011;98: 163704.
31. McDannold N, Arvanitis CD, Vykhodtseva N, Livingstone MS. Temporary disruption of the blood-brain barrier by use of ultrasound and microbubbles: safety and efficacy evaluation in rhesus macaques. Cancer Res 2012;72:3652–63.
32. Hynynen K, McDannold N, Sheikov NA, Jolesz FA, Vykhodtseva N. Local and reversible blood-brain barrier disruption by noninvasive focused ultrasound at frequencies suitable for trans-skull sonications. Neuroimage 2005;24:12–20.
33. Horodyckid C, Canney M, Vignot A, Boisgard R, Drier A, Huberfeld G, et al. Safe long-term repeated disruption of the blood-brain barrier using an implantable ultrasound device: a multiparametric study in a primate model. J Neurosurg 2017;126:1351–61.
34. Idbaih A, Canney M, Belin L, Desseaux C, Vignot A, Bouchoux G, et al. Safety and feasibility of repeated and transient blood-brain barrier disruption by pulsed ultrasound in patients with recurrent glioblastoma. Clin Cancer Res 2019;25: 3793–801.
35. Carpentier A, Canney M, Vignot A, Reina V, Beccaria K, Horodyckid C, et al. Clinical trial of blood-brain barrier disruption by pulsed ultrasound. Sci Transl Med 2016;8:343re2.
36. Abrahao A, Meng Y, Llinas M, Huang Y, Hamani C, Mainprize T, et al. First-in-human trial of blood-brain barrier opening in amyotrophic lateral sclerosis using MR-guided focused ultrasound. Nat Commun 2019;10:4373.
37. Mainprize T, Lipsman N, Huang Y, Meng Y, Bethune A, Ironside S, et al. Blood-brain barrier opening in primary brain tumors with non-invasive MR-guided focused ultrasound: a clinical safety and feasibility study. Sci Rep 2019;9:321.
38. Rezai AR, Ranjan M, D'Haese PF, Haut MW, Carpenter J, Najib U, et al. Noninvasive hippocampal blood-brain barrier opening in Alzheimer's disease with focused ultrasound. Proc Natl Acad Sci U S A 2020;117:9180–2.
39. Beccaria K, Canney M, Goldwirt L, Fernandez C, Piquet J, Perier MC, et al. Ultrasound-induced opening of the blood-brain barrier to enhance temozolomide and irinotecan delivery: an experimental study in rabbits. J Neurosurg 2016; 124:1602–10.
40. Burgess A, Ayala-Grosso CA, Ganguly M, Jordão JF, Aubert I, Hynynen K. Targeted delivery of neural stem cells to the brain using MRI-guided focused ultrasound to disrupt the blood-brain barrier. PLoS One 2011;6:e27877.
41. Belcaid Z, Phallen JA, Zeng J, See AP, Mathios D, Gottschalk C, et al. Focal radiation therapy combined with 4-1BB activation and CTLA-4 blockade yields long-term survival and a protective antigen-specific memory response in a murine glioma model. PLoS One 2014;9:e101764.
42. Reardon DA, Gokhale PC, Klein SR, Ligon KL, Rodig SJ, Ramkissoon SH, et al. Glioblastoma eradication following immune checkpoint blockade in an orthotopic, immunocompetent model. Cancer Immunol Res 2016;4:124–35.
43. Ribas A, Shin DS, Zaretsky J, Frederiksen J, Cornish A, Avramis E, et al. PD-1 blockade expands intratumoral memory T cells. Cancer Immunol Res 2016;4: 194–203.
44. Vom Berg J, Vrohlings M, Haller S, Haimovici A, Kulig P, Sledzinska A, et al. Intratumoral IL-12 combined with CTLA-4 blockade elicits T cell-mediated glioma rejection. J Exp Med 2013;210:2803–11.
45. Louveau A, Smirnov I, Keyes TJ, Eccles JD, Rouhani SJ, Peske JD, et al. Structural and functional features of central nervous system lymphatic vessels. Nature 2015; 523:337–41.
46. Mitchell DA, Batich KA, Gunn MD, Huang MN, Sanchez-Perez L, Nair SK, et al. Tetanus toxoid and CCL3 improve dendritic cell vaccines in mice and glioblastoma patients. Nature 2015;519:366–9.
47. Woroniecka K, Chongsathidkiet P, Rhodin K, Kemeny H, Dechant C, Farber SH, et al. T-cell exhaustion signatures vary with tumor type and are severe in glioblastoma. Clin Cancer Res 2018;24:4175–86.
48. Wherry EJ. T cell exhaustion. Nat Immunol 2011;12:492–9.
49. Wang T, Wang C, Wu J, He C, Zhang W, Liu J, et al. The different T-cell receptor repertoires in breast cancer tumors, draining lymph nodes, and adjacent tissues. Cancer Immunol Res 2017;5:148–56.
50. Reuben A, Gittelman R, Gao J, Zhang J, Yusko EC, Wu CJ, et al. TCR repertoire intratumor heterogeneity in localized lung adenocarcinomas: an association with predicted neoantigen heterogeneity and postsurgical recurrence. Cancer Discov 2017;7:1088–97.
51. Sabins NC, Harman BC, Barone LR, Shen S, Santulli-Marotto S. Differential expression of immune checkpoint modulators on in vitro primed CD4(+) and CD8(+) T cells. Front Immunol 2016;7:221.
52. Kassab C, Zamler D, Gupta P, Srinivasan VM, Rao G, H J, et al. TMIC-60 comprehensive spatial characterization of immune cells in the cns brain tumor microenvironment. Neuro Oncol 2019;21:vi261.
53. Nefedova Y, Cheng P, Gilkes D, Blaskovich M, Beg AA, Sebti SM, et al. Activation of dendritic cells via inhibition of Jak2/STAT3 signaling. J Immunol 2005;175: 4338–46.
54. Ostroumov D, Fekete-Drimusz N, Saborowski M, Kühnel F, Woller N. CD4 and CD8 T lymphocyte interplay in controlling tumor growth. Cell Mol Life Sci 2018; 75:689–713.
55. Fujita M, Zhu X, Ueda R, Sasaki K, Kohanbash G, Kastenhuber ER, et al. Effective immunotherapy against murine gliomas using type 1 polarizing dendritic cells–significant roles of CXCL10. Cancer Res 2009;69:1587–95.
56. Jiang XB, Lu XL, Hu P, Liu RE. Improved therapeutic efficacy using vaccination with glioma lysate-pulsed dendritic cells combined with IP-10 in murine glioma. Vaccine 2009;27:6210–6.
57. Zhu X, Fallert-Junecko BA, Fujita M, Ueda R, Kohanbash G, Kastenhuber ER, et al. Poly-ICLC promotes the infiltration of effector T cells into intracranial gliomas via induction of CXCL10 in IFN-alpha and IFN-gamma dependent manners. Cancer Immunol Immunother 2010;59:1401–9.
58. Koper OM, Kamin´ska J, Sawicki K, Kemona H. CXCL9, CXCL10, CXCL11, and their receptor (CXCR3) in neuroinflammation and neurodegeneration. Adv Clin Exp Med 2018;27:849–56.
59. Karin N, Razon H. Chemokines beyond chemo-attraction: CXCL10 and its significant role in cancer and autoimmunity. Cytokine 2018; 109:24–8.
60. Zumwalt TJ, Arnold M, Goel A, Boland CR. Active secretion of CXCL10 and CCL5 from colorectal cancer microenvironments associates with GranzymeB+ CD8+ T-cell infiltration. Oncotarget 2015;6:2981–91.
61. Barash U, Zohar Y, Wildbaum G, Beider K, Nagler A, Karin N, et al. Heparanase enhances myeloma progression via CXCL10 downregulation. Leukemia 2014;28: 2178–87.
62. Barreira da Silva R, Laird ME, Yatim N, Fiette L, Ingersoll MA, Albert ML. Dipeptidylpeptidase 4 inhibition enhances lymphocyte trafficking, improving both naturally occurring tumor immunity and immunotherapy. Nat Immunol 2015;16:850–8.
63. Park SH, Kim MJ, Jung HH, Chang WS, Choi HS, Rachmilevitch I, et al. Safety and feasibility of multiple blood-brain barrier disruptions for the treatment of glioblastoma in patients undergoing standard adjuvant chemotherapy. J Neurosurg 2020:1–9.
64. O'Reilly MA, Jones RM, Barrett E, Schwab A, Head E, Hynynen K. Investigation of the safety of focused ultrasound-induced blood-brain barrier opening in a natural canine model of aging. Theranostics 2017;7:3573–84.
65. Zhu L, Cheng G, Ye D, Nazeri A, Yue Y, Liu W, et al. Focused ultrasound-enabled brain tumor liquid biopsy. Sci Rep 2018;8:6553.
66. Pacia CP, Zhu L, Yang Y, Yue Y, Nazeri A, Michael Gach H, et al. Feasibility and safety of focused ultrasound-enabled liquid biopsy in the brain of a porcine model. Sci Rep 2020;10:7449.
67. Meng Y, Pople CB, Suppiah S, Llinas M, Huang Y, Sahgal A, et al. MR-guided focused ultrasound liquid biopsy enriches circulating biomarkers in patients with brain tumors. Neuro-oncol 2021.
68. Chen H, Konofagou EE. The size of blood-brain barrier opening induced by focused ultrasound is dictated by the acoustic pressure. J Cereb Blood Flow Metab 2014;34:1197–204.
69. McMahon D, Hynynen K. Acute inflammatory response following increased blood-brain barrier permeability induced by focused ultrasound is dependent on microbubble dose. Theranostics 2017;7:3989–4000.
70. McMahon D, Bendayan R, Hynynen K. Acute effects of focused ultrasound-induced increases in blood-brain barrier permeability on rat microvascular transcriptome. Sci Rep 2017;7:45657.
71. Chapelin F, Gao S, Okada H, Weber TG, Messer K, Ahrens ET. Fluorine-19 nuclear magnetic resonance of chimeric antigen receptor T cell biodistribution in murine cancer model. Sci Rep 2017;7:17748.
72. Zhang H, Wu Y, Wang J, Tang Z, Ren Y, Ni D, et al. In vivo MR imaging of glioma recruitment of adoptive T-cells labeled with NaGdF(4) -TAT nanoprobes. Small 2018;14.

73. Li A, Wu Y, Linnoila J, Pulli B, Wang C, Zeller M, et al. Surface biotinylation of cytotoxic T lymphocytes for in vivo tracking of tumor immunotherapy in murine models. Cancer Immunol Immunother 2016;65:1545–54.
74. Yaghoubi SS, Jensen MC, Satyamurthy N, Budhiraja S, Paik D, Czernin J, et al. Noninvasive detection of therapeutic cytolytic T cells with 18F-FHBG PET in a patient with glioma. Nat Clin Pract Oncol 2009;6:53–8.
75. Lazovic J, Jensen MC, Ferkassian E, Aguilar B, Raubitschek A, Jacobs RE. Imaging immune response in vivo: cytolytic action of genetically altered T cells directed to glioblastoma multiforme. Clin Cancer Res 2008;14:3832–9.
76. Weathers SP, Penas-Prado M, Pei BL, Ling X, Kassab C, Banerjee P, et al. Glioblastoma-mediated immune dysfunction limits CMV-specific T cells and therapeutic responses: results from a phase I/II trial. Clin Cancer Res 2020;26:3565–77.
77. de Groot J, Penas-Prado M, Alfaro-Munoz K, Hunter K, Pei BL, O'Brien B, et al. Window-of-opportunity clinical trial of pembrolizumab in patients with recurrent glioblastoma reveals predominance of immune-suppressive macrophages. Neuro Oncol 2020;22:539–49.
78. O'Rourke DM, Nasrallah MP, Desai A, Melenhorst JJ, Mansfield K, Morrissette JJD, et al. A single dose of peripherally infused EGFRvIII-directed CAR T cells mediates antigen loss and induces adaptive resistance in patients with recurrent glioblastoma. Sci Transl Med 2017;9:eaaa0984.
79. Sampson JH, Heimberger AB, Archer GE, Aldape KD, Friedman AH, Friedman HS, et al. Immunologic escape after prolonged progression-free survival with epidermal growth factor receptor variant III peptide vaccination in patients with newly diagnosed glioblastoma. J Clin Oncol 2010;28:4722–9.